

PAPER • OPEN ACCESS

Distribution of inception times in repetitive pulsed discharges in synthetic air

To cite this article: S Mirpour *et al* 2020 *Plasma Sources Sci. Technol.* **29** 115010

View the [article online](#) for updates and enhancements.



IOP | ebooksTM

Bringing together innovative digital publishing with leading authors from the global scientific community.

Start exploring the collection—download the first chapter of every title for free.

Distribution of inception times in repetitive pulsed discharges in synthetic air

S Mirpour^{1,3,*}, A Martinez^{2,3}, J Teunissen², U Ebert^{1,2}
and S Nijdam¹

¹ Department of Applied Physics, Eindhoven University of Technology, PO Box 513, 5600 MB Eindhoven, The Netherlands

² Centrum Wiskunde & Informatica (CWI), Amsterdam, The Netherlands

E-mail: s.mirpour@tue.nl and Andy.Martinez@cwil.nl

Received 3 June 2020, revised 18 August 2020

Accepted for publication 8 September 2020

Published 11 November 2020



Abstract

Knowing which processes and species are responsible for discharge inception is important for being able to speed up, delay, or completely avoid it. We study discharge inception in 500 mbar synthetic air by applying 10 ms long 17 kV pulses with a repetition frequency of 2 Hz to a pin-to-plate electrode geometry with a gap length of 6 cm. We record inception times for hundreds of pulses by measuring the time delay between the rising edge of the high-voltage (HV) pulse and the signal from a photo-multiplier tube. Three characteristic time scales for inception are observed: (1) 20 ns, (2) 25 μ s, and (3) 125 μ s. To investigate the underlying processes, we apply a low-voltage (LV) pulse in between the HV pulses. These LV pulses can speed up or delay discharge inception, and our results suggest that the three time scales correspond to: (1) free electrons or electron detachment from negative ions close to the electrode, (2) a process that liberates electrons from (quasi)-neutrals, and (3) the drift of an elevated density of negative ions to the ionization zone. However, each of these explanations has its caveats, which we discuss. We present a theoretical analysis of the distribution of inception times, and perform particle simulations in the experimental discharge geometry. Some of the observed phenomena can be explained by these approaches, but a surprising number of open questions remain.

Keywords: discharge inception, streamer, air, delay, repetitive pulse

(Some figures may appear in colour only in the online journal)

1. Introduction

The properties of streamer discharges (velocity, electric field at the tip, electron/ion densities in the body and at the tip, branching, etc) have been widely studied, see e.g. [1–9]. Streamers are important in various fields like high-voltage (HV) engineering, atmospheric discharge phenomena (e.g. lightning),

etc. The streamer inception voltage and the influence of the voltage rise time on this inception voltage were studied in [10–12]. Briels *et al* [13] used time resolved optical measurements to investigate the inception of positive streamers in air. The analysis was focussed on the streamer inception voltage and the reduced streamer diameter. Nevertheless, the current understanding of the complex interplay of factors governing streamer inception is still very limited. In the present work we investigate the streamer inception process in more detail.

As shown in figure 1, a positive streamer discharge can start when the electric field around a conductor or dielectric rises, free electrons move opposite to this field and travel towards positively charged tips or electrodes. When these

³ These authors contributed equally.

*Author to whom any correspondence should be addressed.



Original content from this work may be used under the terms of the [Creative Commons Attribution 4.0 licence](https://creativecommons.org/licenses/by/4.0/). Any further distribution of this work must maintain attribution to the author(s) and the title of the work, journal citation and DOI.

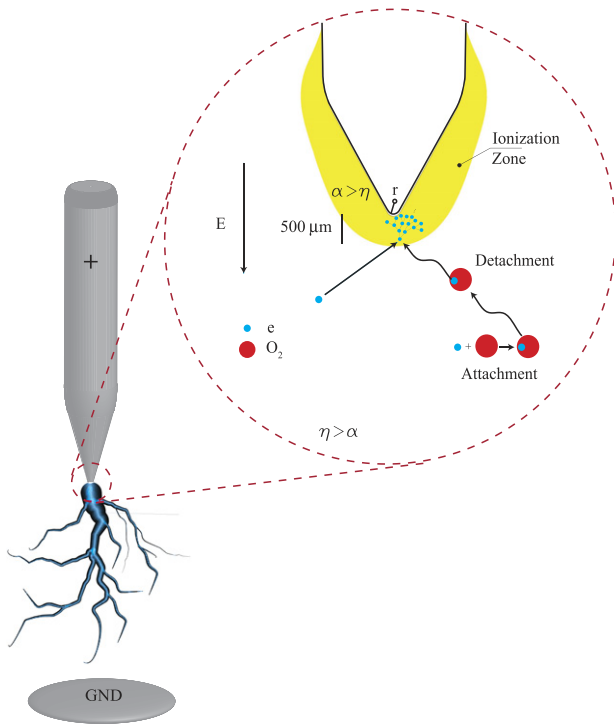


Figure 1. The inception process in which a free electron or an electron detached from a negative ion can enter the ionization zone and trigger the inception process (not to scale, $r = 100 \mu\text{m}$). α and η represent the ionization and attachment coefficient respectively.

electrons enter a region where the electron impact ionization rate is greater than the electron attachment rate they can form an avalanche. The electrons replicate rapidly due to direct impact ionization until the electron density becomes so high that space charge effects become important. The avalanche(s) can then transform into a streamer discharge. The so-called Meek criterion [14, 15] is an estimate for the number of electrons required for this avalanche-to-streamer transition.

We can identify several questions related to streamer inception: where do the streamer-starting electrons come from? What can the inception time between an applied HV and the start of the streamer discharge tell us? Are there ways to manipulate the inception of a streamer discharge without changing quantities like pressure, gas composition, applied HV? Answers to these questions can be useful in HV engineering applications where the inception of streamer discharges is unwanted or better control over the streamer development is needed. Somewhat related is a more poorly understood fundamental question [16, 17]: how does lightning initiate inside thunderstorms when the background electric field is below breakdown? A big difference with lightning inception and repetitive pulse discharge inception is that lightning inception is not a repetitive process. Nevertheless, answering the posed questions in a lab setting with a repetitive pulse is a first

step towards better understanding of the lightning inception process.

Streamer-starting electrons can be provided by a cosmic ray ionization event, by radioactivity from surrounding material, by gas specific electron sources, and by charges in the gap leftover from previous discharges. For N_2/O_2 -mixtures, processes like detachment from O_2^- and O^- [18–20], can provide electrons to start a streamer discharge. Li *et al* [21] investigated how the time between two HV pulses influences positive streamer inception and propagation. It was found that for short times between two HV pulses positive streamers starting on the second pulse would follow the paths of the streamers developed during the first pulse. The general physical mechanism is understood, but the mechanism that provides electrons for these second-pulse streamers is not clear yet.

The time delay between applying an HV pulse to an electrode and the inception of a streamer discharge was investigated by Wang and Geng [11]. They split the streamer inception time into two components: the time to reach the inception voltage, and a statistical time delay due to the random nature of having an electron in the right circumstances to trigger a discharge. They conclude that the density and lifetime of O_2^- are the two main factors that determine the statistical delay, and that the statistical delay using a positive lightning impulse voltage follows a Rayleigh distribution.

Fengbo *et al* [22] investigated the voltage recovery rate in spark gaps. They developed a repetitive nanosecond pulse source and found that by applying a +1 kV DC bias between two high voltage pulses to their trigger electrode they could reduce the effect of residual electrons in the discharge gap. This reduction increased the voltage recovery rate of the pulse source. Moreover, they showed that a higher DC bias voltage does not change the voltage recovery rate because of the shielding effect around the electrode. Zhao and Li [23] investigated the influence of memory effect agents on the streamer evolution in a nanosecond repetitive discharge. They showed that by applying a superimposed DC voltage bias the number of pulses required to get breakdown is reduced. This is further reduced by increasing the DC bias until a minimum is reached. They stated that at high HV repetition frequency the electrons are attracted towards the anode by a positive DC bias. At low repetition frequency, they showed that the number of pulses before breakdown decreases. Also, they observed that the inception moment is delayed under a negative DC voltage bias.

In this work, we have taken these prior investigations as a basis for new advanced experiments and numerical models. These will give a more detailed insight into the relevant mechanisms and species involved in the inception of repetitively pulsed discharges in synthetic air. We experimentally studied the statistical distribution of the inception time (t_{inc}) and how this distribution can be manipulated. We have

detected three distinct peaks in the distribution of t_{inc} which implies three different processes for triggering a discharge in the experiment.

We also found that the histogram of inception times t_{inc} could be manipulated by applying a low-voltage (LV) pulse between two HV pulses. This LV pulse influenced the residual charged species in the discharge gap. This method allowed further investigations of the processes responsible for each peak in the t_{inc} histogram. We investigate possible sources of the three peaks: free electrons or quickly detached electrons from negative ions, Penning ionization, and drift of negative ions to the ionization zone.

A particle model for the electrons with Monte-Carlo based collision sampling (MCC) was used to further substantiate the arguments made for the sources of each peak in the t_{inc} histogram. The particle model is described in [24] except that in the current investigation of the avalanche phase, the electric field does not change in time. We have also tracked O_2^- as particles drifting in the electric field and eventually detaching electrons.

This paper is organized as follows: in section 2 we describe the experimental setup, applied conditions, and diagnostic methods. Section 3 discusses estimates of initial conditions for the simulation model. Section 4 explains the simulation model. Section 5 shows the results and discussion of the baseline experiment and different variations of the LV pulse parameters (polarity, width, and time between it and the HV pulse). Finally, in section 6 we summarize the paper and list the open questions.

2. Experimental setup

2.1. Experimental conditions

All experiments in this study are performed with a point-to-plane electrode geometry (shown in figure 2) in which the electrodes are separated by a distance of 60 mm. The powered electrode, anode (with a tip radius of about $100 \mu\text{m}$), is connected to the HV circuit which consists of an HV solid state push-pull switch (Behlke HTS 301-10-GSM) and a 200 pF capacitor. This produces voltage pulses with amplitudes of 17 kV, pulse widths of 10 ms, and rise times of about 40 ns. The pulses were applied with a repetition rate of 2 Hz. We chose this frequency to have a shorter acquisition time. The background pressure level in the vessel was 1 mbar and the working pressure was 500 mbar. Synthetic air (80% N_2 + 20% O_2) with less than 1 ppm impurity was used. The humidity level outside of the vessel was measured at around 47%. During the entire experimental period the vessel was kept closed. We have not seen any noticeable changes in the tip curvature and the obtained results were well reproducible.

To study how residual charges influence the streamer inception, in most experiments we applied an LV pulse between each two HV pulses. This was possible via a second custom-built push-pull switch which can apply a bias to the negative side of the HV switch. With that, we were able to make a bias with variable voltage (V_b), width ($t_{\text{LV-dur}}$), and time before the HV pulse ($t_{\text{LV-sep}}$). In the case of $t_{\text{LV-sep}} = 0$, the LV pulse attaches

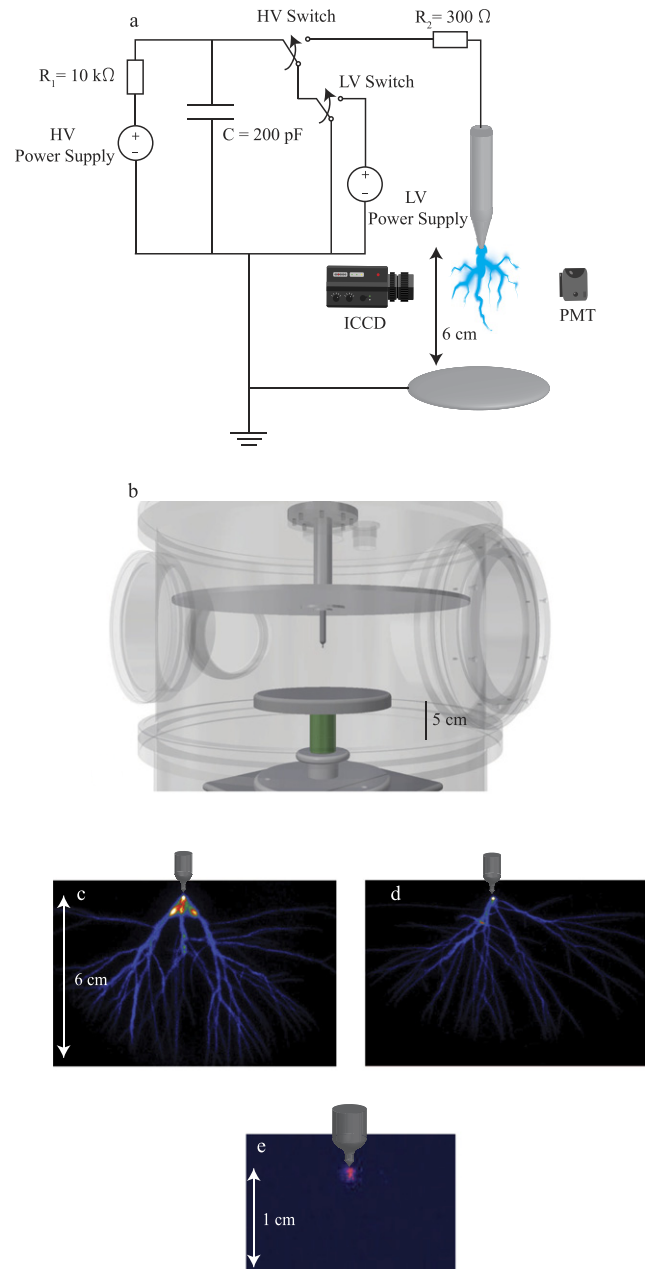


Figure 2. (a) Schematic view of experimental setup with HV power supply connected to the anode (not to scale). (b) schematic of experimental vessel. The large disc above the anode tip is a Teflon disc to separate the HV from the top of the vessel. (c)–(e) Discharges in 500 mbar synthetic air with HV amplitude of 17 kV and repetition rate of 2 Hz. (c) Without applying LV pulse, (d) with applying positive LV pulse $t_{\text{LV-sep}} = 0$ and $t_{\text{LV-dur}} = 50$ ms. The gate time of the camera is $10 \mu\text{s}$. (e) Glow observed after a streamer burst, the glow lasts for the remaining duration of the HV pulse.

to the HV pulse. The applied V_b was always plus or minus 300 V.

2.2. Measuring inception time t_{inc}

A photo-multiplier tube (PMT, Hamamatsu H6779-04) was placed behind a window of the vessel to capture photons produced by the discharge around the anode tip. The PMT has a response time of less than 1 ns and can measure the photons emitted in the inception process. The output signal

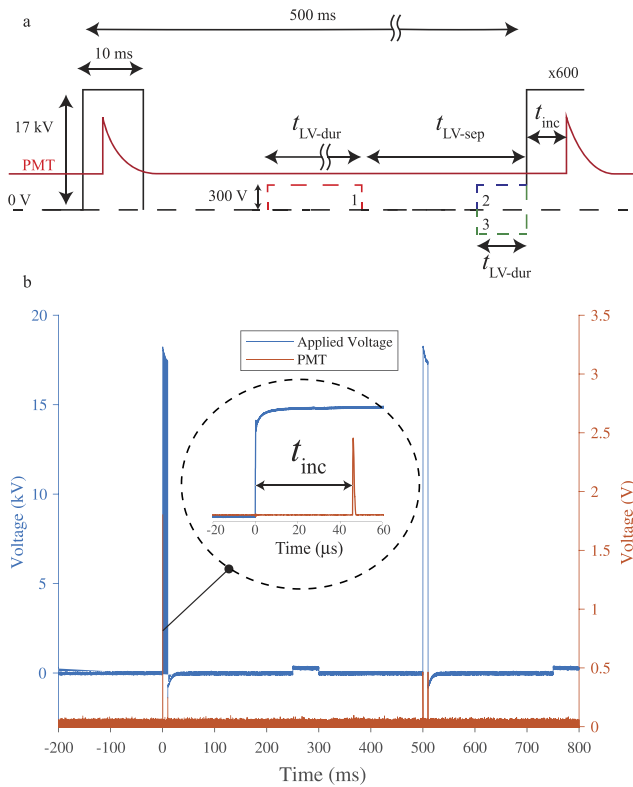


Figure 3. (a) Scheme of applied HV pulse with three different LV pulse configurations: 1. Positive LV pulse between two HV pulses (red) 2. Positive LV pulse attached to the HV pulse (blue) and 3. Negative LV pulse attached to the HV pulse (green). (b) Typical applied HV and LV voltage with PMT signal output.

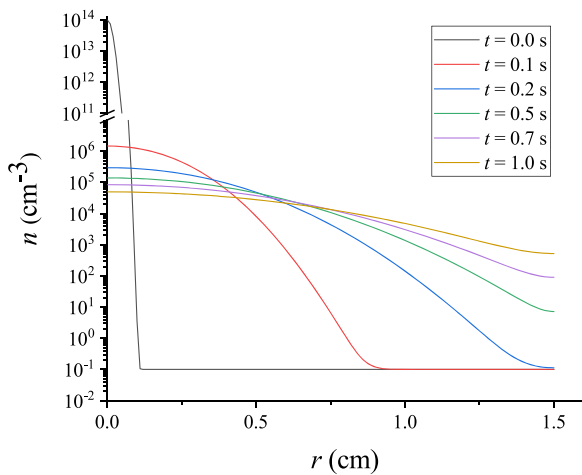


Figure 4. Ionization density n_i as a function of radius r for different times t after the streamer discharge, as described in the text.

was collected by a 12 bit HD 6104 Teledyne Lecroy oscilloscope with a maximum sample rate of 50 MS s^{-1} . Such a measurement was generally done for 600 cycles per setting. We consistently observed only one inception for each 10 ms HV pulse. From these results we established for each cycle the temporal delay between the moment the HV pulse reaches 10% of its maximum and the moment that the PMT reaches 10% of its maximum, which would indicate streamer

Table 1. Reactions included in the particle model with $M = \text{N}_2$ or O_2 . Cross sections were taken from the Itikawa database [30, 31, 32]. (\diamond) 3-body attachment was taken from the Phelps database [33] and was only taken into account for the case where O_2 is the third body. According to reaction rates for 3-body attachment reported in [34] the 3-body attachment with O_2 as third body is almost 50 times higher than with N_2 as the third body. (*) Elastic momentum transfer cross sections were taken from the Itikawa database to use as elastic scattering cross sections. Since the particle model only has isotropic elastic scattering this is a valid approximation to make. (*) All excitation reactions for N_2 and O_2 which were listed in the Itikawa database [30] were taken into account; listing them here would clutter the reaction list. (\ddagger) Photo-ionization was included using a stochastic version of Zheleznyak's model [35], as was done before in [24, 36]. (Δ) The detachment reaction rate was taken from [19].

Elastic	$e^- + \text{N}_2 \rightarrow e^- + \text{N}_2$ (*)
	$e^- + \text{O}_2 \rightarrow e^- + \text{O}_2$ (*)
Ionization	$e^- + \text{N}_2 \rightarrow 2e^- + \text{N}_2^+$
	$e^- + \text{N}_2 \rightarrow 2e^- + \text{N}^+ + \text{N}$
	$e^- + \text{N}_2 \rightarrow 3e^- + \text{N}^{2+} + \text{N}$
	$e^- + \text{O}_2 \rightarrow 2e^- + \text{O}_2^+$
	$e^- + \text{O}_2 \rightarrow 2e^- + \text{O}^+ + \text{O}$
	$e^- + \text{O}_2 \rightarrow 3e^- + \text{O}^{2+} + \text{O}$
Attachment	$e^- + \text{O}_2 + \text{O}_2 \rightarrow \text{O}_2^- + \text{O}_2$ (\diamond)
	$e^- + \text{O}_2 \rightarrow \text{O}^- + \text{O}$
Excitation	$e^- + \text{O}_2 \rightarrow (*)$
	$e^- + \text{N}_2 \rightarrow (*)$
Photo-ionization (\ddagger)	(1) $e^- + \text{N}_2 \rightarrow e^- + \text{N}_2^*$
	(2) $\text{N}_2^* \rightarrow \text{N}_2 + \gamma$
	(3) $\gamma + \text{O}_2 \rightarrow e^- + \text{O}_2^+$
Detachment (Δ)	$\text{O}_2^- + M \rightarrow \text{O}_2 + e^- + M$

inception. We call this temporal delay the inception time t_{inc} and have indicated it in figure 3. The estimated total error in t_{inc} is less than 5 ns. Next, a histogram of the t_{inc} values was made. For histograms with logarithmic bins we used a binning function which divided the data into 700 bins in a logarithmic scale starting from 10 ns to the logarithm of the maximum of the t_{inc} (with the MATLAB function of `logspace(log10(0.01), log10(max(data)), 700)`), and for the linear bin histogram (figure 13) we divided the data into 100 bins. Note that for low-time bins the histogram is sparsely filled due to the limitation of the oscilloscope memory in long-acquisition windows. This results in a coarser effective bin spacing for these conditions.

2.3. ICCD imaging of streamers

An intensified CCD (ICCD, Andor Technology iStar) with nanosecond gate and a Nikkor UV 105 mm lens $f/4.5$ was used to image the discharges. The images presented in figure 2(c)–(e) are rendered in a false-colour scale for clarity.

The criterion used for detecting streamer inception is the moment when the PMT shows a peak which is three times higher than the average background noise. Note that the very first few pulses after starting the experiment were not included in the measurements to avoid any start-up effects. We found that in all cases exactly one discharge inception event per HV cycle was observed. This means that the discharge inception probability was 100% for all experiments done. The criterion for streamer inception detection was tested using the ICCD camera. In all cases, we found that whenever the PMT detected

streamer inception, the ICCD images also showed a developed streamer. The images also show that most of the streamers reach the grounded electrode (see below).

Every time an experimental parameter was varied (pressure, applied voltage, pulse duration, etc) the system was evacuated to a background pressure of about 1 mbar and then refilled with synthetic air. This procedure removed any species produced by preceding experiments.

3. Estimate of initial conditions

Figure 2(c) and (d) shows ICCD images of streamers with and without applying an LV pulse. The inception cloud, which has been introduced in [13], is smaller when an LV pulse with $t_{LV-sep} = 0$ and $t_{LV-dur} = 50$ ms is applied before the HV pulse. Note that later we will discuss that after the application of such a positive 50 ms LV pulse (see figure 11(e)) most discharges occur during the rise-time of the HV pulse, i.e., within the first inception peak (to be defined later). Based on these observations, we may conclude that the negative ions which accumulate around the anode during the LV pulse initiate the discharge faster and hence the inception cloud breaks up already during the rise-time of the HV pulse, and hence stays smaller, as the maximal radius is given by voltage over break-down field [13]. A more comprehensive explanation will be given in the coming section. Except for this observation, no significant differences in streamer propagation and branching were found in the streamer images with or without application of an LV pulse. There were also no differences observed between the images of streamers initiated in the first, second, and third peak.

After the streamer burst we observed a DC glow (figure 2(e)), often called Hermstein glow [25], which lasts during the remaining duration of the HV pulse and uniformly covered the powered electrode tip [26]. The DC glow contains negative charges, screens the local electric field near the electrode tip, and prevents the onset of a new streamer. Generally, the DC glow together with the streamer channel leave ions and excited species behind which can play a significant role in the emergence of streamers during the next HV pulse.

Here we estimate the density and distribution of the ions left behind by a streamer channel at the beginning of the next HV pulse. Electrons are not taken into account in this estimation (and future simulations) since they will attach very quickly after they have been produced (see also figure 8). At ground level the majority of background ionization is produced by radioactive decay [27], mainly by radon which produces alpha particles which in turn create electron-ion pairs by disintegration. This process can produce a background ionization level of 10^3 – 10^4 cm⁻³ (predominantly in the form of positive and negative ions). Since we perform our experiments in a metallic vessel which stops alpha particles after tens of μ m, the background ionization due to radon decay inside the experimental vessel will be substantially lower. Cosmic ray ionization events can still occur inside the metallic vessel, but for the free electrons to have an effect on the discharge inception, before they become attached, they would need to be present in the small ionization zone around the HV pin electrode (yellow zone in

figure 3) at the moment the HV pulse is turned on (or before the attachment time on the order of ns).

Following the arguments in [28], the ion density changes due to diffusion and recombination

$$\partial_t n_i = D_{ion} \cdot \nabla^2 n_i - k_{rec} \cdot n_i^2 \quad (1)$$

where n_i denotes the density of both positive and negative ions, and net charges and electric fields are neglected. $D_{ion} = 0.1$ cm² s⁻¹ and $k_{rec} = 2.6 \times 10^{-6}$ cm³ s⁻¹ are diffusion coefficient and recombination rate at 500 mbar in air, respectively [28]. Note that we assumed that the positive and negative ion densities are equal. It is possible that there may be a small or local imbalance in charged species densities which would be able to severely affect the recombination rate. The initial condition for this equation consists of a Gaussian streamer channel centred around $r = 0$ with $n_i = n_{channel} \cdot e^{-r^2/R^2}$ with $n_{channel} = 10^{14}$ cm⁻³ and $R = 0.3$ mm, and an initial background ionization of 0.1 cm⁻³. These values are derived from an actual streamer observed by an ICCD camera and described in [28]. Figure 4 shows this estimated initial ion density after the end of the HV pulse as $t = 0$ and its temporal evolution under diffusion and recombination until the next HV pulse at $t = 0.5$ s. Within these 0.5 s between the pulses, the ionization density decreases to about 10^5 cm⁻³ on the streamer axis and the spatial profile becomes wider due to diffusion. The ionization density stays approximately constant up to a radius of 0.5 cm. (We remark that we used $\partial_r n_i = 0$ as a boundary condition at $r = 1.5$ cm, which imitates the next streamer channel being at 3 cm distance).

The calculated initial ion density of 10^5 cm⁻³ is several orders of magnitude larger than the largest initial O₂⁻ ion density of 10 cm⁻³ used in the simulations presented in this paper. The results for these simulations are shown in figure 14(c) and will be discussed in a later section. The main point to be discussed here is that if a density of 10 cm⁻³ (or larger) is used as an initial homogeneous O₂⁻ ion density, all inception times t_{inc} are smaller than 1 μ s which does not match with experiments.

A possible explanation for this discrepancy is the formation of O₃⁻ and NO₃⁻. Popov [29] has shown that already after 10 ms of diffusive expansion of a streamer channel in air at atmospheric pressure the main negative ions are O₃⁻ and NO₃⁻ with other ions like O₂⁻ having a substantially lower contribution to the total negative ion density. O₃⁻ and NO₃⁻ have an electron bonding energy 4 and 7 times higher than O₂⁻ respectively. This means that detachment from these negative ions does not occur as easily as from O₂⁻.

O₃⁻ and NO₃⁻ will serve as an effective electron sink. The result is that when the next HV pulse is applied, only a small fraction of negative ions (mainly the O₂⁻ ions) will be able to detach an electron which can initiate the discharge. Further chemical modelling is needed to investigate this in the future.

4. Simulation model

4.1. Particle model

We have developed a particle model to simulate the inception behaviour. In this model, electrons and negative oxygen ions

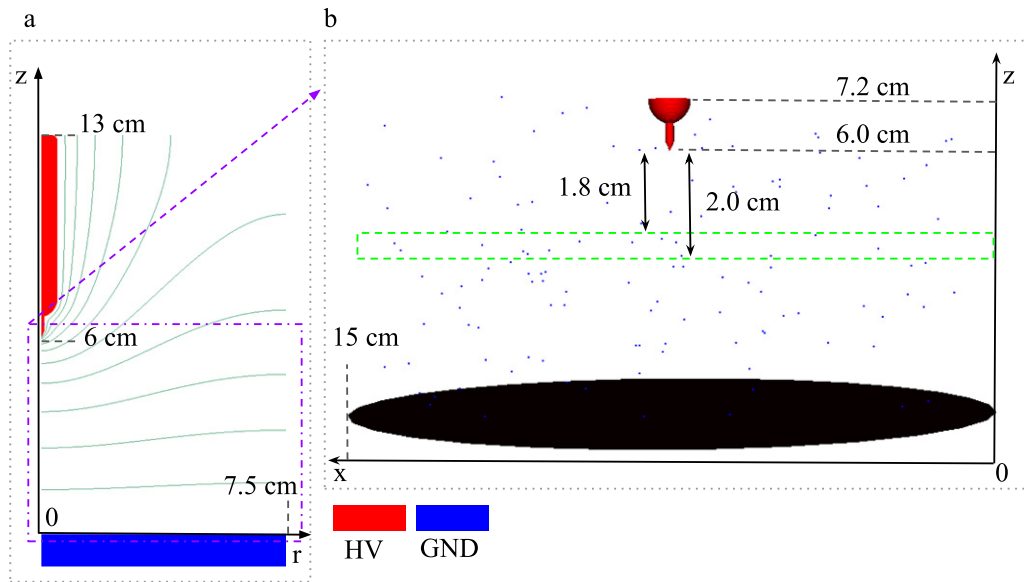


Figure 5. The computational domain for (a) the electric field computation with COMSOL (included are scalar potential contour lines), and (b) the particle model. The COMSOL domain uses cylindrical coordinates while the particle model uses 3D Cartesian coordinates in a box of $15 \times 15 \times 7.2 \text{ cm}^3$. The coloured spheres in (b) represent O_2^- ions placed homogeneously in the simulation box (in this particular figure a density of 0.1 cm^{-3} was used which equals 128 ions). The green highlighted area represents the position where an inhomogeneous distribution of O_2^- ions was placed in some simulations to obtain the histograms in figure 14(d).

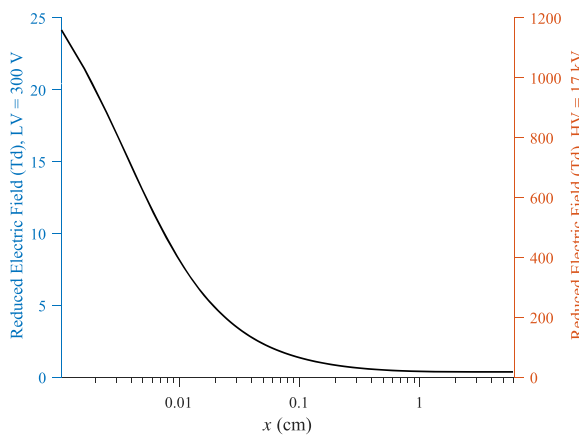


Figure 6. The reduced electric field E/N (where N is the gas number density) in Townsend on the axis of the gap for 500 mbar synthetic air at 300 K. Blue (left) y-axis shows the values for an applied potential of 300 V, red (right) y-axis shows the values for an applied potential of 17 kV. The maximum reduced electric field at the tip of the pin electrode ($x = 0$) was 24 Td for 300 V applied and close to 1200 Td for 17 kV applied. The bottom grounded electrode is at $x = 6 \text{ cm}$.

(O_2^-) are tracked as particles moving through a constant background of N_2 and O_2 molecules under the influence of the local electric field. Table 1 shows the plasma-chemical reactions included in the model; they include electron impact ionization, electron attachment and detachment and photo-ionization.

The electrons were moved with a 3D particle model using a MCC technique, as described in [24], to take collisions with the neutral background gas into account. A Velocity Verlet scheme was used to advance the electrons. The axisymmetric electric field was kept static throughout the simulations. This field was interpolated to the particle positions by

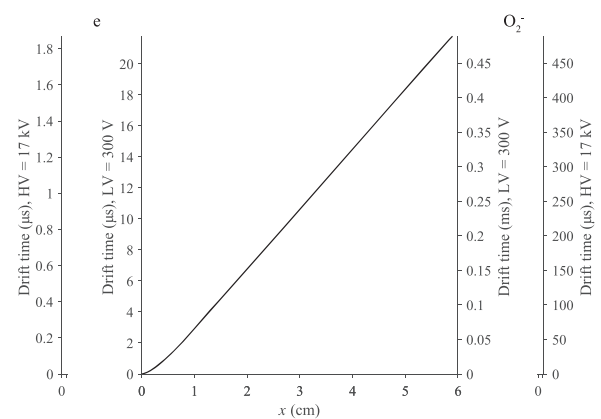


Figure 7. Drift time on the axis of symmetry of an electron (left) or an O_2^- ion (right) from a distance x to the pointed electrode at $x = 0$ when a voltage of 300 V (inner y-axis) or 17 kV (outer y-axis) is applied across the gap. Calculated using (2). Only a single line is drawn because the different mobilities and voltages only change the slope of the drift time curves which can be reflected in the y-axis scale.

converting the Cartesian particle coordinates (x, y, z) to (r, z) coordinates.

The availability of cross sections for O_2^- collisions with neutral gas molecules is limited. The motion of these ions was therefore modelled by using a mobility coefficient μ . Their drift velocity is then given by $\mathbf{v} = -\mu\mathbf{E}$, where \mathbf{E} is the electric field at the location of the O_2^- ion. This drift approximation was deemed acceptable since the O_2^- ions only serve as an electron source through detachment.

The mobility of O_2^- as a function of the reduced electric field was taken from the VIEHLAND database [37]. This mobility is reported for air at STP conditions and was scaled to

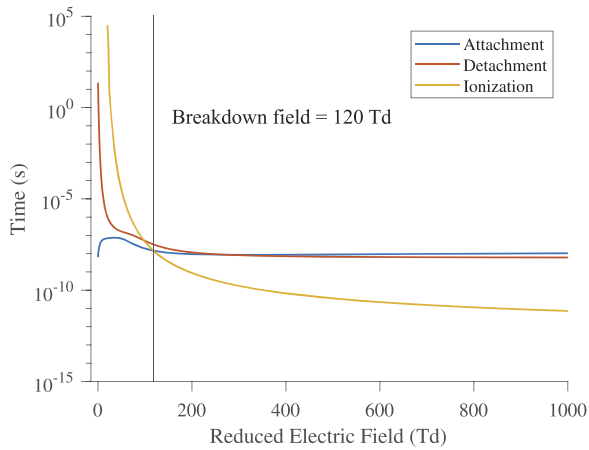


Figure 8. Attachment, detachment and ionization time of electrons in an 80/20 N_2/O_2 mixture at 500 mbar. The detachment time from O_2^- was calculated from formulas given in [19]. The attachment and ionization time was calculated from cross sections of Itikawa [30–32] and for the 3-body attachment from Phelps [33] which were input into BOLSIG- [40, 41] to calculate reaction rates.

a pressure of 500 mbar using $\mu = \mu_{STP} \frac{N_{STP}}{N}$, with μ and μ_{STP} the mobility at 500 mbar and at 1 bar respectively, and N and N_{STP} the number density of the gas at 500 mbar and at 1 bar respectively. This tabulated database was linearly interpolated to obtain mobilities corresponding to electric fields which are not explicitly included in the database.

Experimentally measured detachment rates were fitted by Pancheshnyi [19] to obtain the following approximation for the electron detachment rate from O_2^- : $r = N_{gas} k_0 \exp \frac{-\Delta\epsilon}{\theta}$. Here, N_{gas} is the number density of the gas, and $k_0 = (1.22 \pm 0.07) 10^{-11} \text{ cm}^3 \text{ s}^{-1}$ and $\Delta\epsilon = 0.78 \pm 0.03 \text{ eV}$ are the fit parameters used for the Arrhenius approximation. Furthermore, θ is the effective ion temperature calculated as $\theta = \frac{\pi}{2} m_{ion} v_{ion}^2 + k_B T_{gas}$ where m_{ion} and v_{ion} are the mass and velocity of the ion respectively, k_B is Boltzmann's constant and T_{gas} is the temperature of the gas. The detachment rate is used as a collision frequency for the O_2^- -ions so that the null collision method can be used to stochastically determine if a detachment reaction takes places in a given timestep for a given O_2^- -ion.

4.2. Electric field

The electrode geometry, shown in figure 5(a), was drawn in a CAD programme according to the dimensions of the experimentally used electrode. To calculate the electric field distribution, this CAD drawn electrode geometry was imported into COMSOL [38] where the cylindrical symmetry of the problem was used. The boundary conditions for the scalar potential ϕ were set to: $\frac{\partial\phi}{\partial r}|_{r=0} = 0$, $\frac{\partial\phi}{\partial r}|_{r=7.5\text{cm}} = 0$, $\frac{\partial\phi}{\partial z}|_{z=13\text{cm}} = 0$, $\phi|_{z=0} = 0$, and $\phi|_{pin} = V$ (where V is the applied voltage to the pin electrode). The rise time of the experimentally used voltage source was not taken into account in the simulations. Since we only have negative ions as initial condition in section 3 the rise time of tens of ns would not have a substantial effect. In choosing these boundary conditions we neglected the influence of the Teflon disc above the needle electrode at $z = 13 \text{ cm}$. Because the Teflon disc is so far away from the discharge

region and the dielectric constant of Teflon is only around 2, we can assume that it would not influence the discharge considerably. The reduced electric field on the axis of the discharge gap is shown in figure 6, for the case of an applied voltage of 300 V (the LV pulse) and of 17 kV (the HV pulse).

This electric field was imported into the particle model and assumed to remain constant in time during the inception phase, i.e., space-charge effects as they occur later in the streamer phase are neglected. The simulation domain is shown in figure 5(b); it is a cube of $15 \times 15 \times 7.2 \text{ cm}^3$ which completely covers the 15 cm diameter grounded electrode and the full discharge gap.

4.3. Inception time t_{inc}

In the experiments, the inception time t_{inc} was measured as the time from the application of the high voltage pulse until the time of light emission from the discharge. In the simulations, the presence of 10^6 electrons was used to determine the moment of inception, as was also done in previous inception simulations [39]. We assume the presence of 10^6 electrons indicates rapid and continued discharge growth, due to additional electron avalanches caused by photo-ionization.

4.4. Drift and reaction times

To guide the interpretation of the experimental results, we here discuss relevant drift and reaction times.

Figure 7 shows the drift time $t_{drift}(x)$ of electrons and O_2^- ions from a distance x to the pointed electrode at $x = 0$ on the axis of symmetry. It is calculated as

$$t_{drift}(x) = \int_0^x \frac{1}{\mu(E)E(x')} dx', \quad (2)$$

where μ is the mobility of the respective species, and $E(x)$ the electric field on the axis, see figure 6. The two axes on the left of figure 7 show the drift time of electrons either in the HV of 17 kV or in the LV of 300 V, and the two axes on the right show the same for O_2^- ions, in the inverse order of LV and HV. To cross the gap of 6 cm on the axis of symmetry, electrons need around $1.8 \mu\text{s}$ under HV conditions and $20 \mu\text{s}$ under LV conditions, and O_2^- ions need around $490 \mu\text{s}$ (HV) and 27.5 ms (LV).

The charged species do not only drift in the field, but they also react, and characteristic times for electrons as a function of reduced electric field are plotted in figure 8, namely the attachment time, the detachment time and the impact ionization time as a function of the reduced electric field. The breakdown field is indicated as well; for higher fields electron avalanches grow.

5. Results and discussion

5.1. Baseline experiment

In our baseline experiment, we applied HV pulses of 17 kV with a duration of 10 ms to artificial air at 500 mbar, and we repeated this 6000 times with a repetition frequency of 2 Hz.

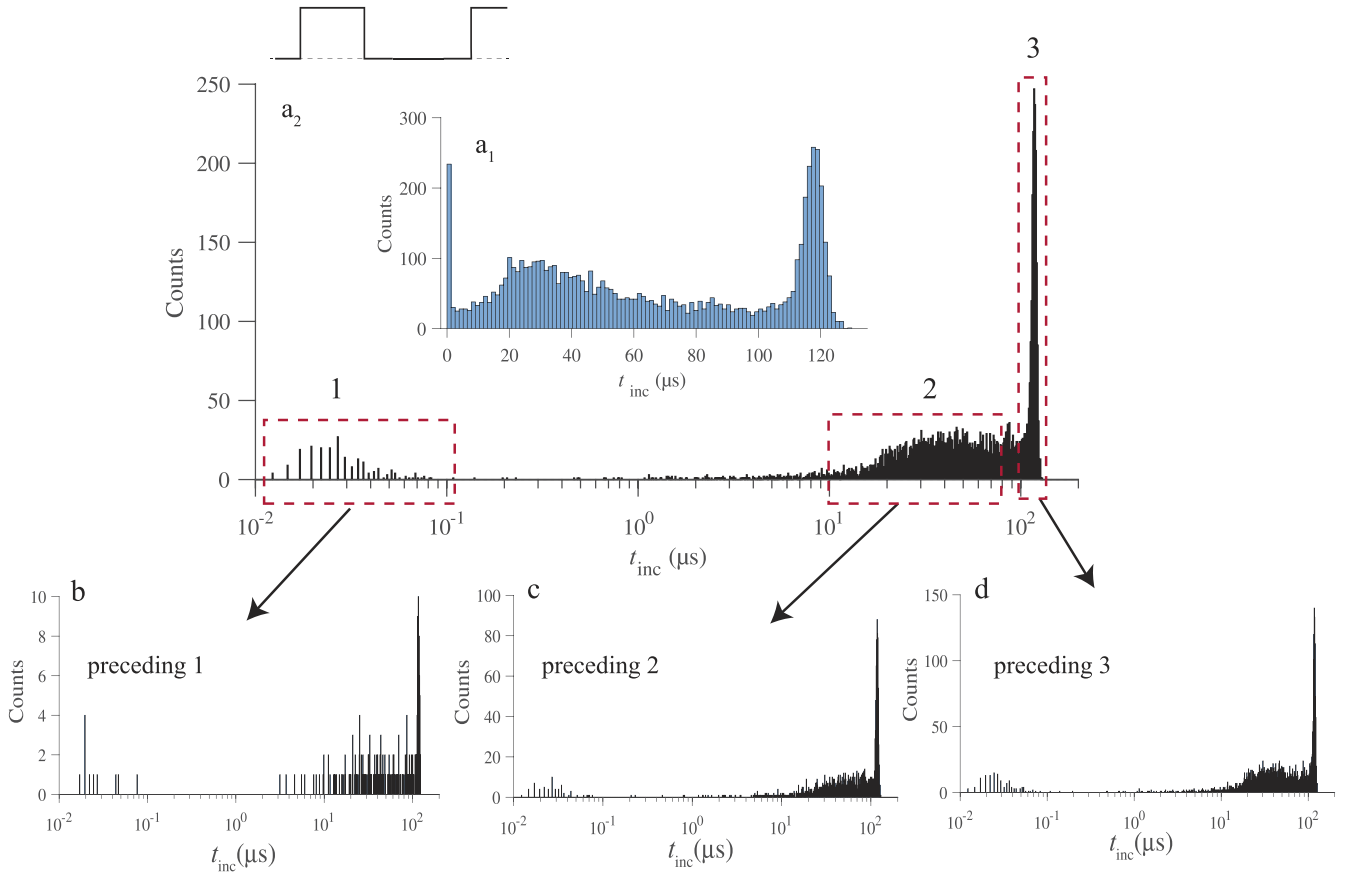


Figure 9. Histogram of discharge inception times t_{inc} with a_1 linear and a_2 logarithmic bins for 6000 discharges in the baseline experiment. For the logarithmic plot the bin size scales with $\log t$, but note that for the smallest timescales most bins are empty due to sparse oscilloscope sampling. The graph in the upper left corner of panel (a) indicates the voltage wave form, a sequence of high voltage pulses. The graphs in the second row show the histogram of t_{inc} for the pulse preceding (b) the first peak, (c) the second peak, and (d) the third peak. The contribution of the first, second, and third peak is 3.4%, 60.9%, and 31.8%, respectively. Note that the second peak is not covering all of the data between the first and the third peak.

The histogram of inception times t_{inc} is displayed in figure 9(a) on a logarithmic scale for the time, where the size of the time bins is scaled as $\log t$. The histogram shows that there are three distinct peaks in this distribution, namely at around 20 ns, 25 μs , and 125 μs . The aim of the paper is to study the conditions for these three peaks to form and to understand their physical nature as far as possible—though puzzles remain.

It is clear that a discharge starts from an impact ionization avalanche of electrons in the high field zone near the pin electrode. And our simulations confirm that one initial electron in this region can start sufficient electron multiplication to start a discharge, at least when it is initially near the symmetry axis of the set-up. So the relevant question is: where do these initial electrons come from, when and how many? And the fact that there are three distinct inception time peaks suggests, that there might be three distinct sources for these electrons.

In a first step, we have checked whether there is any temporal correlation between discharges of the three different peaks. Figure 9(b) shows the t_{inc} histogram for the discharges immediately before a discharge with a t_{inc} in the first peak, and panels c and d show the same for the second and third peak. We see that the histograms in figure 9(b)–(d) all retain the same structure as the baseline figure 9(a), up to differences

due to the different total number of discharges. This means that the inception times t_{inc} for two consecutive discharges are uncorrelated.

5.2. Baseline theory

Before embarking into a more detailed discussion of the experiments, let us first state what we expect in the simplest case: a homogeneous distribution either of electrons or of O_2^- ions.

Let us assume in a first step that electron reactions like impact ionization or attachment as well as electron diffusion can be neglected. In this case the electron flux \mathbf{j} in an electric field \mathbf{E} is $\mathbf{j} = \mu_e(E)\mathbf{E} n_e$ where n_e is the electron density. We can neglect space charge effects on the inception process itself because space charge densities of such magnitudes that they have a significant effect on the electric field contradict with the observed stochastic behaviour of the inception delay. If the mobility μ_e does not depend on the electric field, and if there are no space charges $\nabla \cdot \mathbf{E} = 0$, then a homogeneous electron density will stay homogeneous while drifting in the field, as

$$\partial_t n_e = -\nabla \cdot \mathbf{j} = -\nabla \cdot (\mu_e \mathbf{E} n_e) = 0, \quad (3)$$

according to the conservation law of electrons and to the

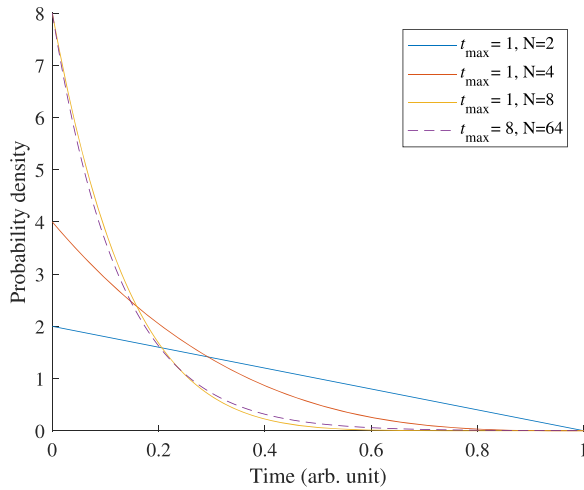


Figure 10. Analytic estimate of the inception probability versus time as given by equation (4). N represents the initial number of particles and t_{\max} their maximal drift time to the electrode, see the text for details. Note that the inception probability depends, to a good approximation, on the ratio N/t_{\max} . Surprisingly, our experimental results do not resemble the curves shown here.

assumptions above. This means that at any moment in time the same flux of electrons passes at any point in space, independently of the precise electric field configuration. In particular, the electron flux arriving at the high field zone near the electrode is constant in time.

As shown in appendix A, the probability density of inception can then be approximated by

$$f(t) = N/t_{\max}(1 - t/t_{\max})^{N-1}, \quad (4)$$

where N denotes the initial number of electrons (or O_2^- ions) equally distributed in some volume around the electrode and t_{\max} is the maximal drift time of these particles towards the electrode. As discussed in appendix A, equation (4) depends to a good approximation on the ratio N/t_{\max} , which can be interpreted as the number of particles reaching the electrode per unit time. Figure 10 illustrates the dependence of equation (4) on N and t_{\max} . In all cases, the probability of inception decreases with time, but this happens more rapidly for larger values of N/t_{\max} . The mean inception time given by equation (4) is $t_{\max}/(N+1)$; this time scale decreases approximately like the inverse of N/t_{\max} .

The above analysis applies to both electrons and O_2^- ions, but with a longer time scale for O_2^- ions due to their smaller mobility. These ions will drift in the field until they reach the high field zone, where they detach an electron that can start an avalanche and a discharge. In the experiments, we expect to have mostly negative ions at the beginning of the HV pulse, since the time scale for electron attachment in the absence of an electric field is on the order of 10 ns, see figure 8.

Comparing the analytical estimate for the histogram of inception times t_{inc} in figure 10 with the experimentally observed histogram in figure 9 we see that there is a strong deviation from the analytical estimate, with three peaks in the distribution rather than one continuous decrease. Therefore at

least one of the assumptions above must be wrong. This could for example happen when:

- There is more than one species involved.
- The species are initially not homogeneously distributed.
- Attachment or ionization reactions cannot be neglected along the path of the charged species or there is another reaction liberating or binding free electrons under specific conditions.
- There are space charge effects, hence $\nabla \cdot \mathbf{E} \neq 0$.
- The mobility of the species is strongly field dependent.

In the following sections we will discuss each peak in the distribution of inception times, and how and why they deviate from the analytical estimate above.

5.3. The first peak

In the inception time histogram, shown in figure 9(a) with a statistics over 6000 discharges, the first peak occurs between 10 ns and 100 ns which is several orders of magnitude earlier and shorter than the two other peaks. The first peak accounts for about 3.4% of all inception events.

There are essentially two possible sources for this early peak: either free electrons are already available when the HV pulse starts, or there are particles, e.g., O_2^- ions, that rapidly release electrons at that moment.

Electrons are quite unlikely to be present at the beginning of the HV pulse, since according to figure 8 they attach to oxygen on a timescale of 10–100 ns for electric fields well below the breakdown value. Therefore electrons produced during a previous HV pulse will attach between the pulses. It is reasonable to assume that free electrons already present in the gap when an HV pulse is applied were not produced by a previous discharge, but by rare events like cosmic rays or radioactive decay of materials present in the lab.

O_2^- -ions could be a source of free electrons as figure 8 shows that a detachment time smaller than 100 ns occurs for a reduced electric field larger than 120 Td. Figure 6 shows that this reduced electric field is found for distances smaller than 0.06 cm from the pin electrode when a potential of 17 kV is applied. This shows that ions very close to the pin electrode can detach an electron sufficiently rapidly to produce the first peak. The region of space extending to a distance of 0.06 cm will be called the active zone for the rest of the discussion of the first peak. The following discussion will assume O_2^- -ions to be the main contributor to the discharges belonging to the first peak (in principle any detaching negative ion can contribute to the discharge inception, but for our experimental conditions O_2^- will be the most prevalent [19]).

5.3.1. Hypothesis: electrons detaching from O_2^- in the active zone as the source of the first peak. To test whether O_2^- -ions were present before an HV pulse, we applied a positive LV pulse of 300 V with a duration of $t_{\text{LV-dur}} = 1$ ms or longer and immediately before the HV pulse ($t_{\text{LV-sep}} = 0$). The goal was to pull all negative ions in the gap towards the pin electrode during the LV pulse without triggering a discharge.

The histogram of inception times for 600 repetitions of the pulse experiment is shown in figure 11(b); it shows that the first

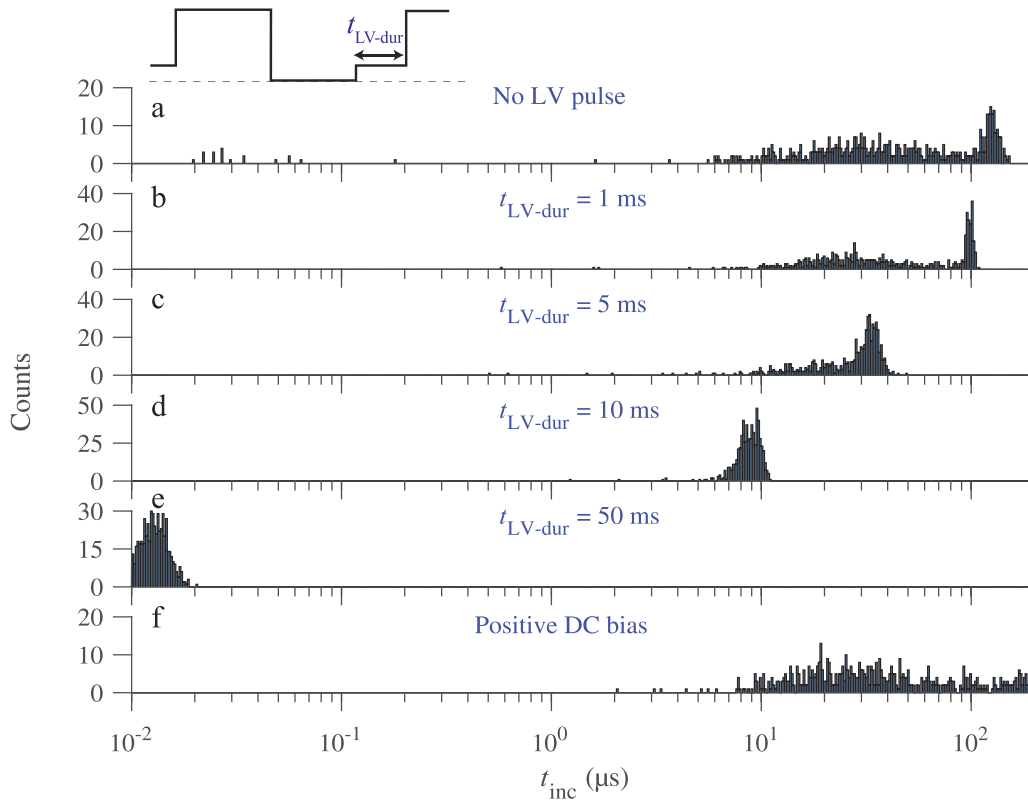


Figure 11. Histograms of discharge inception time t_{inc} for 600 discharges produced (a) for no LV pulse and by applying a 300 V pulse for $t_{\text{LV-dur}} =$ (b) 1, (c) 5, (d) 10, and (e) 50 ms, (f) a DC bias before a 17 kV pulse of 10 ms with a repetition frequency of 2 Hz.

peak is removed. The removal of the first peak can be explained in the following manner: as O_2^- -ions are drawn closer to the electrode at a certain point they will be too close to the surface of the electrode for a detached electron to produce a large enough avalanche to initiate a discharge.

A new question arises when we follow this reasoning: why would not O_2^- coming from further in the discharge gap ‘replace’ the O_2^- that are now pulled too close to the pin electrode and thus keep the first peak unchanged? This can only happen if the density of O_2^- -ions is higher in the active zone than in the region of space from which O_2^- -ions could travel towards this active zone during the LV pulse. It remains unsolved as to what would cause such a difference in O_2^- density. A possible source of a higher density of O_2^- ions close to the pin electrode could be the continuous glow discharge observed after a discharge has been triggered but before the HV pulse is turned off. This glow discharge has been discussed in section 3.

Figure 12 shows the effects that a -300 V LV pulse has on the t_{inc} histogram. For any duration $t_{\text{LV-dur}}$ (1 ms, 5 ms, 10 ms, 50 ms, and DC) of the LV pulse, O_2^- should drift out of the active zone according to the calculated drift times in figure 7. This would mean that the first peak should not be present anymore in the t_{inc} histogram or be shifted to higher t_{inc} accounting for the drift time of O_2^- -ions. Figures 12(b)–(f) shows that the first peak remains present for times below 100 ns, just as without an LV pulse.

A possible explanation is that the electric field off-axis of the discharge gap is much lower which would keep at least

some O_2^- -ions in the active zone during a negative LV pulse. This is a reasonable explanation for the short LV pulses ($t_{\text{LV-sep}} \leq 10$ ms), but should still not be able to explain the results for $t_{\text{LV-sep}} = 50$ ms or negative DC.

Another explanation can be the emission of electrons from the electrode due to impact/absorption of the positive ions. The kinetic energy of the positive ions will be much lower than the work function of the electrode, but if the positive ions are in a more energetic state (increased internal energy) then a surface reaction might occur which emits an electron.

5.4. The second peak

5.4.1. Experimental evaluation. The second peak in the inception time histogram in figure 9 occurs around $25 \mu\text{s}$. We re-plot this data in figure 13(a) in a linear scale to better investigate this source of discharge inception. The results of applying a positive or negative LV pulse, with different $t_{\text{LV-dur}}$, before the HV pulse ($t_{\text{LV-sep}} = 0$) are plotted on a linear scale in figures 13(b)–(f).

We see in figures 13(b)–(f) that the second peak does not shift significantly to lower or higher t_{inc} . The first and third peak shift substantially more and, in figure 13(d), the shifted third peak ‘eats up’ part of the second peak. These results suggest that the source of the second peak is not measurably influenced by the electric field produced by the LV pulse.

For one set of 600 discharges we decreased the repetition frequency of the HV pulses to 0.2 Hz to investigate its effects on the second peak. Figure 17(a) shows the effect that this repetition frequency change had on t_{inc} . We see that decreasing

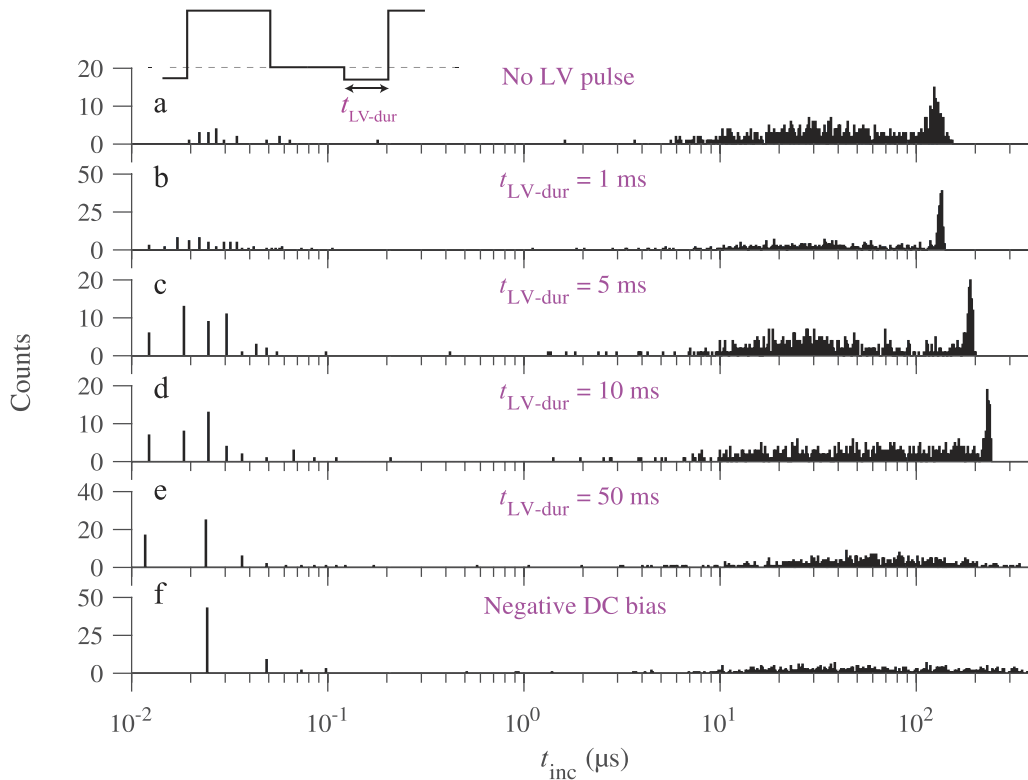


Figure 12. Histograms of discharge inception time t_{inc} for 600 discharges produced by applying a -300 V pulse for $t_{\text{LV-dur}} =$ (b) 1, (c) 5, (d) 10, and (e) 50 ms, for (a) no LV pulse and (f) a DC bias before a 17 kV pulse of 10 ms with a repetition frequency of 2 Hz. Note: the y-axis of each histogram is different which can give the impression that the first peak strongly changes in height depending on $t_{\text{LV-dur}}$ which it does not.

Table 2. Table with experimentally observed shifts (Δt_{inc}) of the third peak in the t_{inc} histograms shown in figure 12 when applying an LV pulse with variable $t_{\text{LV-dur}}$. If the t_{inc} of the third peak corresponds to the drift time of O_2^- ions then x_{start} would be the average starting position of the O_2^- ions. The shift in starting position due to the LV pulse is represented by Δx_{start} . The distance that O_2^- can travel during the LV pulse is calculated using equation (2) and represented here as Δx_{LV} .

$t_{\text{LV-dur}}$ (ms)	t_{inc} (μs)	Δt_{inc} (μs)	x_{start} (cm)	Δx_{start} (cm)	Δx_{LV} (cm)
Positive LV					
0	122.8		1.73		
1	98.3	24.5	1.45	0.28	0.20
5	32.52	90.28	0.66	1.07	1.04
10	9.1	113.7	0.3	1.43	>1.73
Negative LV					
0	122.8		1.73		
1	132.3	-9.5	1.84	-0.11	-0.2
5	184.6	-61.8	2.45	-0.72	-1.03
10	228.3	-105.5	2.95	-1.22	-2.02

the repetition frequency causes the first and third peak to completely disappear while keeping the second peak intact. The source of the second peak seems to be able to live for at least 5 s without an applied electric field.

We would also like to remark that we had to open up the vessel once for maintenance. When we closed the vessel and pumped the pressure down to 500 mbar, the second peak was completely removed from the t_{inc} histogram. After pumping

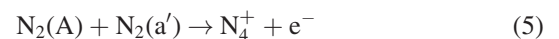
the vessel down for a week we measured the t_{inc} histogram again and found the histogram as in figure 9 again. We think that by opening the vessel we allowed H_2O to enter the vessel. From [42] we know that H_2O is an effective quencher of excited O_2 and N_2 states which could correspond with the removal of the second peak. Since H_2O is not easily pumped out of the vessel we required a week to obtain the original synthetic air composition of 80% N_2 and 20% O_2 .

In the following section we will discuss several hypotheses which could explain the different experimental observations about the source of the second peak (No measurable effect of an LV pulse, only peak which remains when the repetition frequency is reduced to 0.2 Hz, and removal of only this peak when the vessel was briefly opened).

5.4.2. Hypothesis. The first peak has been argued in the previous section to be caused by discharge inception by free electrons or O_2^- already present in the discharge gap when the HV pulse is applied (or created shortly thereafter).

Since the first peak is influenced strongly by applying an LV pulse before the HV pulse and the second peak is not, we think it is likely that the second peak is caused by electron creation processes involving only neutral species.

One hypothesis would be the production of electrons due to Penning ionization. We worked in an N_2/O_2 gas mixture so we can identify various Penning ionization reactions from literature [43]:



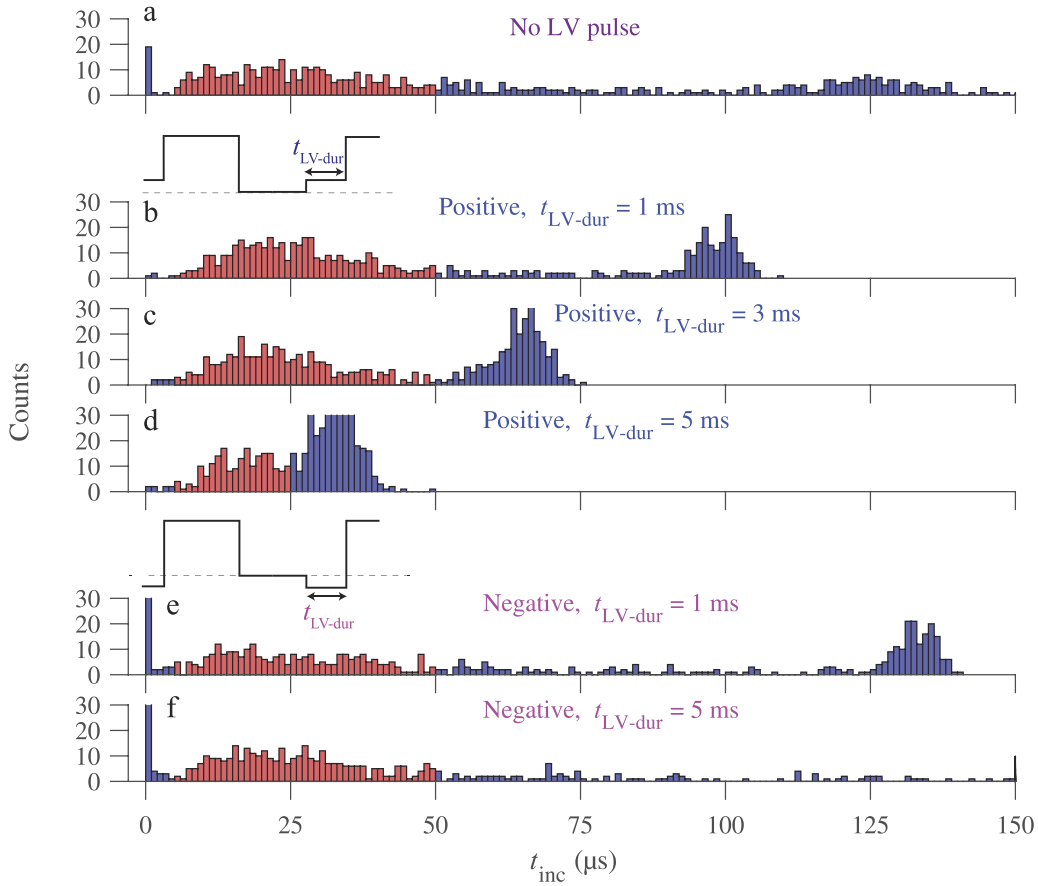
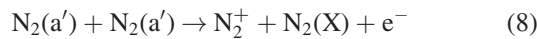
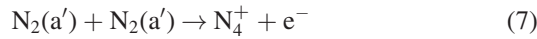
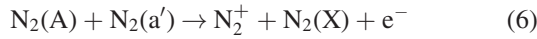


Figure 13. Characterization of second peak (red bars) after applying positive (b–d) and negative (e and f) LV pulses with 300 V amplitude and varying t_{LV-dur} . Note: the peaks of this histogram are clipped at 30 counts. This figure is mainly to show relative shifts of the second peak to the other peaks. For absolute counts refer to figures 11 and 12.



However, the lifetime of the excited states $N_2(A)$ and $N_2(a')$ are determined by quenching reactions with O_2 as shown in [44]. At a pressure of 500 mbar these quenching reactions will have a timescale on the order of 10–100 ns. Taking these quenching reactions into account we can assume that the density of $N_2(A)$ and $N_2(a')$ will be very low after the 100 s of ms that the HV pulse was off and thus cannot explain the second peak.

Another possible explanation for the second peak could be that there are quasi-neutral patches of charged species which, due to their space charge effects, cannot be pulled apart by the field created by the LV pulse (or DC), but the large charge densities required for this are not consistent with the observed stochastic inception behaviour.

5.5. The third peak

5.5.1. Source of electrons. The third peak in the baseline experiment occurs around 125 μs . The histogram obtained when we applied a 300 V pulse for 1 ms before the HV pulse, shown in figure 11(b), shows that the third peak shifted to

lower t_{inc} . This shift can mean one of two things: either the source of electrons shifts closer to the electrode, or the process to produce an electron is sped up.

Theoretical results obtained by assuming that the third peak is caused by a source of electrons which can move due to the application of an LV pulse match well with the experimental observations. For this reason the following analysis will start from this assumption.

5.5.2. Hypothesis: drift time of O_2^- as the characteristic time of the third peak. Assuming that the inception time for the third peak is caused by the drift time of a negative ion (e.g. O_2^-) we can calculate whether the shift of the third peak, when applying a positive LV pulse, corresponds to the movement of negative ions during the positive voltage pulse. In the following calculations the drift of the negative ions is calculated directly on the axis of the pin electrode. The electric field will be slightly different off-axis and so results will change when ions are allowed to drift off-axis.

Without a positive LV pulse the third peak occurs at 122.8 μs . We assume that this is the average drift time of an O_2^- ion to get to the HV pin electrode. In principle it is sufficient for the negative ions to travel to the ionization zone, but for calculation purposes it is easier to take the HV pin electrode as endpoint. We therefore find the distance Δx from the HV electrode at which the negative ions start by applying

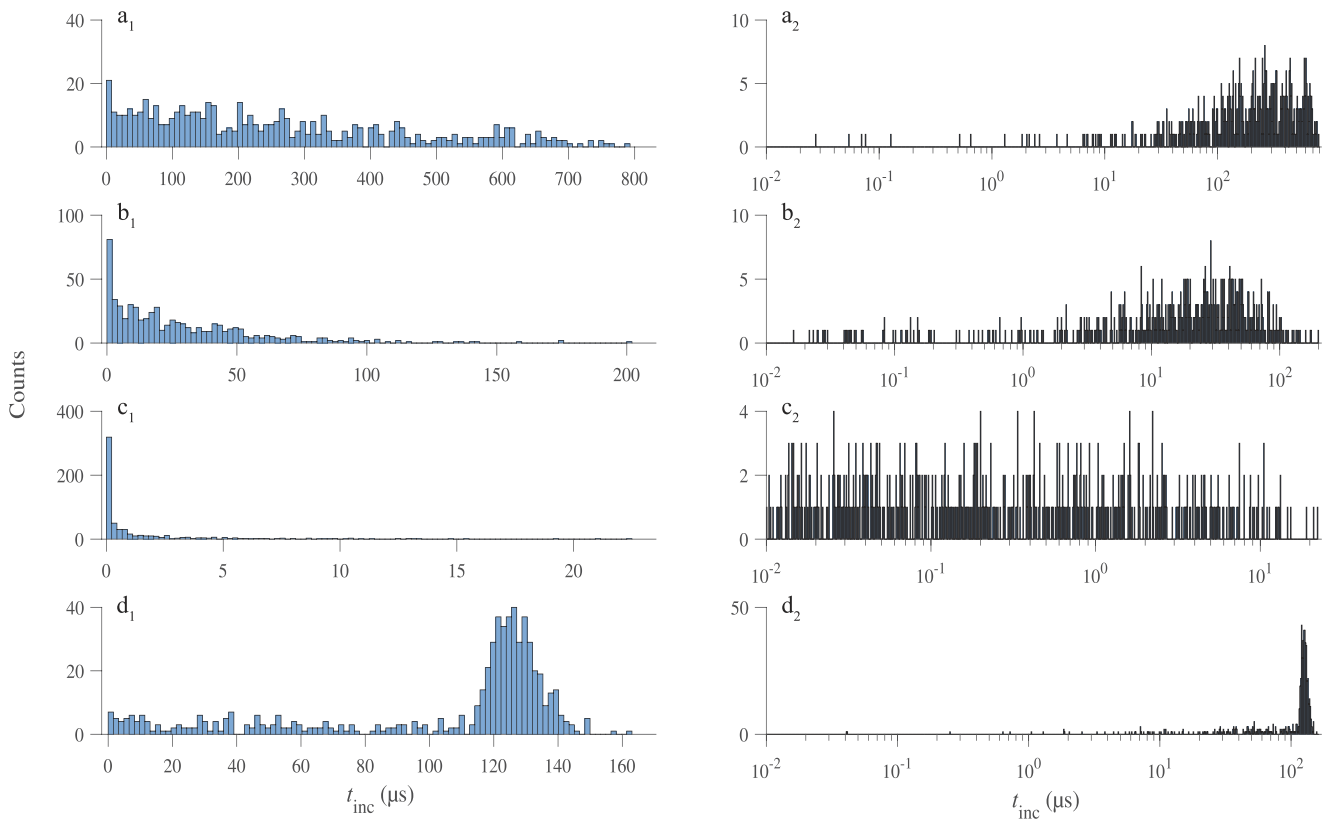


Figure 14. Histograms of t_{inc} from particle simulations with a sample size of 600. Histograms on the same row depict the same simulation results but left side is linear and right side is logarithmic. The initial homogeneous density of O_2^- -ions were: (a) 0.1 cm^{-3} ($N = 124$), (b) 1 cm^{-3} ($N = 1238$), (c) 10 cm^{-3} ($N = 12364$), and (d) 0.1 cm^{-3} ($N = 124$) with an extra patch of O_2^- -ions ($N = 354$) placed between 1.8 cm and 2.0 cm from the pin electrode (green highlighted area in figure 5). All simulations have an inception probability of 1 except for (a) which has an inception probability of 0.92.

equation (2), where t_{inc} is the average inception time of $122.8 \mu\text{s}$, $E(x)$ is the applied electric field between the electrodes (on the axis), and $\mu_1(E(x))$ is the O_2^- -ion mobility at 500 mbar at position x . We obtain $\Delta x = 1.73 \text{ cm}$. This means that if the inception time of $122.8 \mu\text{s}$ of the third peak is caused by the drift time of negative ions to the HV electrode, they would need to have started at a distance of 1.73 cm from the pin electrode.

When we applied a positive LV pulse with $t_{\text{LV-dur}} = 1 \text{ ms}$ and $t_{\text{LV-sep}} = 0$, the third peak shifted to $98.3 \mu\text{s}$. Performing the same calculation as before, we find that the negative ions started at a distance of 1.45 cm from the HV pin electrode. Indicating that during the LV pulse the negative ions moved 0.28 cm towards the pin electrode.

Now we can calculate the distance that an O_2^- -ion would travel during this LV pulse. Starting from a position of 1.73 cm from the pin electrode the O_2^- -ion will drift for a time $t_{\text{LV-dur}}$ in the field of the LV pulse. In this case $t_{\text{LV-dur}} = 1 \text{ ms}$ and using equation (2) we find $\Delta x = 0.20 \text{ cm}$.

We see that the difference in travel distance ($1.73 \text{ cm} - 1.45 \text{ cm} = 0.28 \text{ cm}$) of the negative ions for the experiments with and without this positive LV pulse corresponds to the distance O_2^- -ions can travel during this LV pulse (0.20 cm). These calculations suggest that O_2^- -ions cause the third peak and that the values of t_{inc} correspond to the average drift time of the O_2^- -ions to the HV pin electrode.

A comparison of the shift of the third peak caused by the application of a positive LV pulse with various $t_{\text{LV-dur}}$ and the distance negative ions can travel during this LV pulse is given in table 2. In this table we can observe that for $t_{\text{LV-dur}} = 10 \text{ ms}$ the O_2^- -ions should have already reached the pin electrode, but their starting position seems to still be 0.3 cm from the pin electrode. A possible explanation is that the electric field of the LV pulse is not the only force in the gap. Space charge effects could reduce the distance that the negative ions can drift in the field of the LV pulse.

We also applied a negative LV pulse with various $t_{\text{LV-dur}}$ and $t_{\text{LV-sep}} = 0$. Figure 12(e) shows the histogram obtained from these experiments. We can see that the third peak is now shifted to higher t_{inc} . Table 2 shows the experimental and calculated shifts of the third peak for different $t_{\text{LV-dur}}$. We can see that the calculated shifts match pretty well with the experimentally observed shifts. The presented results seem to agree with the idea that the third peak is mainly caused by the drift of negative ions, likely to be O_2^- -ions.

Note that there is a sharp drop after the third peak of around $125 \mu\text{s}$. An interpretation could be that up to a distance of around 1.7 cm there are sufficient negative ions to have a near unity probability of inception. The results should not be interpreted as if there are no ions after this distance of 1.7 cm, they simply do not get a chance to be the cause of inception.

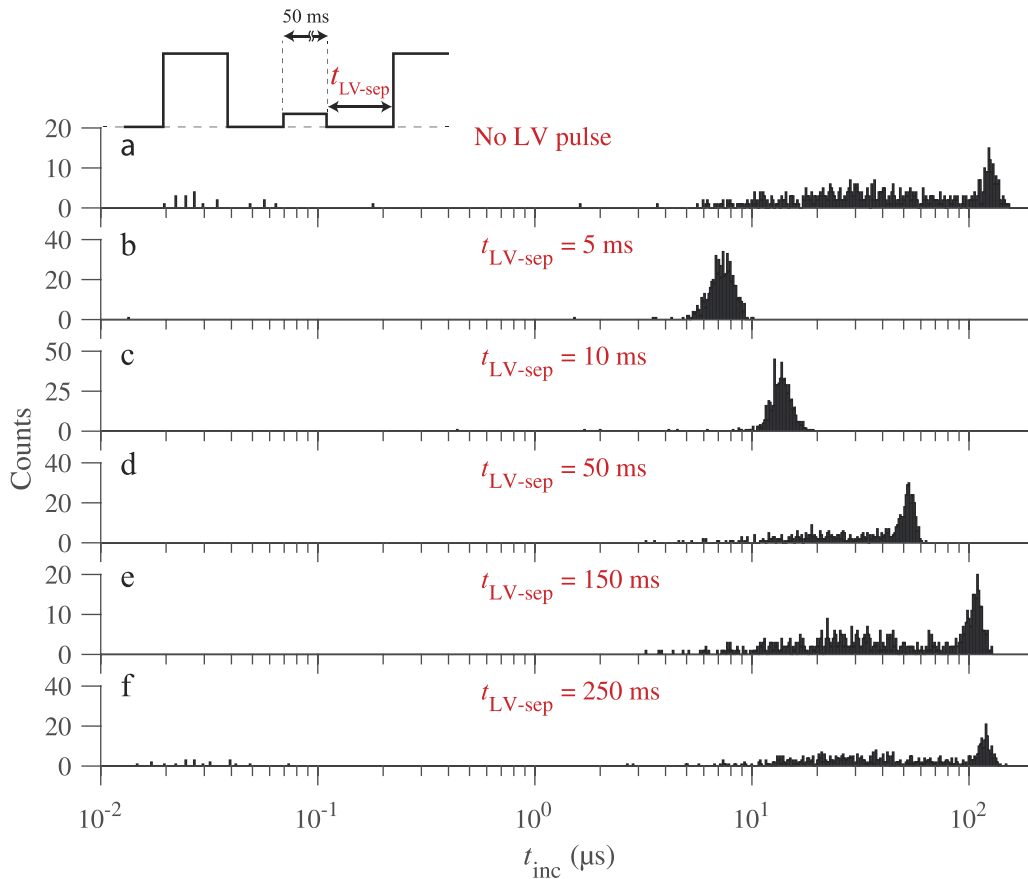


Figure 15. Histograms of discharge inception time t_{inc} for 600 discharges produced by applying a 300 V pulse for 50 ms and $t_{\text{LV-sep}} =$ (b) 5, (c) 10, (d) 50, (e) 150, (f) 250 ms before a 17 kV pulse of 10 ms with a repetition frequency of 2 Hz.

5.5.3. Producing the third peak. Here, we discuss how the third peak appears in linear and log scaled histograms of t_{inc} obtained from particle simulations with different initial conditions. The goal is to understand what the initial conditions of the particle simulations have to be to obtain a comparable result to experiment. Homogeneous ion densities of 0.1 cm^{-3} to 10 cm^{-3} were used as initial conditions. Only O_2^- -ions were placed since from figure 8 we can see that most electrons should have attached already during the 490 ms HV pulse off-time. A fourth particle simulation was done where a homogeneous ion density of 10 cm^{-3} was placed together with an extra patch of ions at a distance of around 1.9 cm from the pin electrode as shown as the green rectangle in figure 5. This extra patch of ions contained 3 times as many ions as in the rest of the domain (124 in the domain, 354 in the extra patch). Each initial condition was run 600 times to obtain statistics on t_{inc} from the simulation results. An initial homogeneous distribution of 0.1 cm^{-3} O_2^- resulted in a probability of inception within 1 ms of 91%, all other initial conditions had a 100% inception chance.

We can see in all initially homogeneous cases that the experimentally observed peak around $125 \mu\text{s}$ is absent from the linear scaled histograms shown in figures 14(a)–(c).

The log scaled histogram shown in figure 14(a₂) contains a peak $>125 \mu\text{s}$ which would naively be matched with the third

peak observed in figure 9. A property of the log scaled histogram is that the bins on the x -axis increase in size as we move along the x -axis. This property causes a peak to show up in log scaled histograms fairly easily. However, note that in the experimental observations of the third peak, it is also visible on a linear scale.

For these simulations there was only one assumption which was that the initial ion density was distributed homogeneously. Since we are investigating the discharge inception for repetitive pulses it is possible that the initial density for the next pulse is not homogeneously distributed. Figure 2(c) shows a typical discharge during one of the HV pulses. We can see that it is not unreasonable to assume an initial inhomogeneous distribution of ions as we move away from the HV pin electrode.

Figure 14(d) shows the histograms of t_{inc} for the simulations with an extra patch of O_2^- -ions placed between 1.8 cm and 2.0 cm from the pin electrode. Due to this inhomogeneous distribution of O_2^- -ions we can see in these histograms that a peak is not only present in the logarithmic scale but also in the linear histogram.

From these results it seems that some inhomogeneity in the spatial distribution of O_2^- -ions is needed to produce the experimentally observed third peak in the histogram of t_{inc} .

5.5.4. Increasing duration between LV and HV pulse. In this section we investigate the influence of increasing the time between the LV pulse and the next HV pulse. We apply an

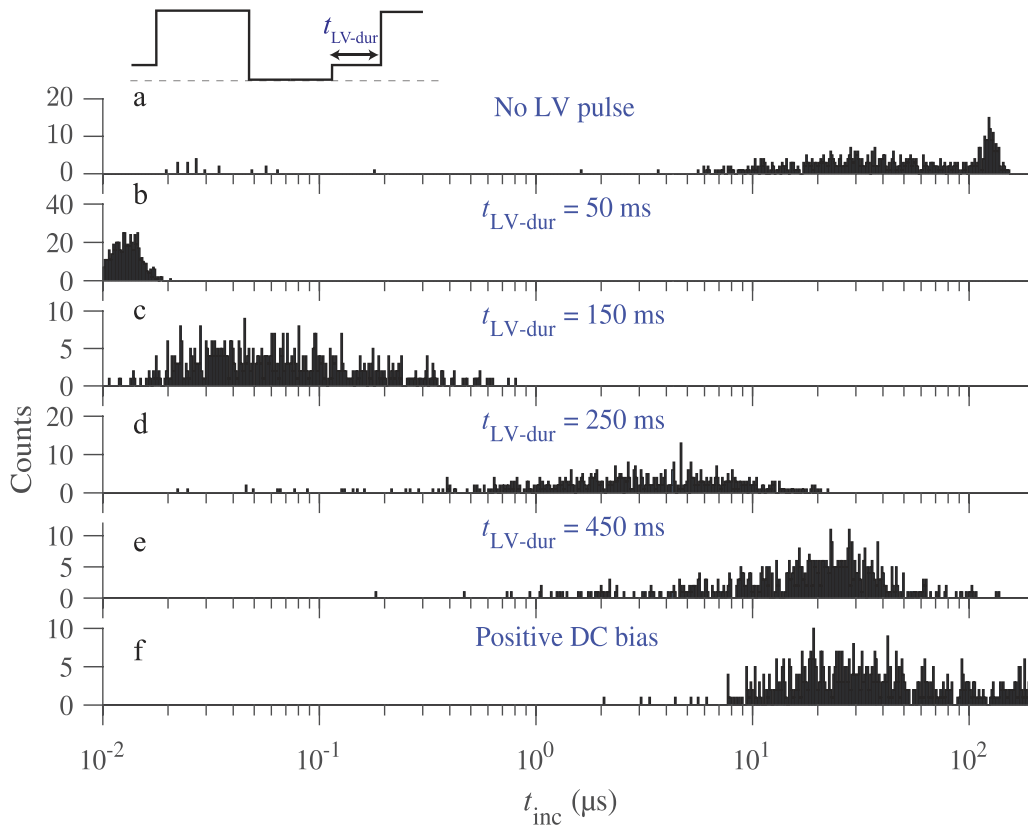


Figure 16. Histograms of discharge inception time t_{inc} for 600 discharges produced by applying a 300 V pulse for $t_{\text{LV-dur}} =$ (b) 50, (c) 150, (d) 250, and (e) 450 ms, for (a) no LV pulse and (f) a DC bias before a 17 kV pulse of 10 ms with a repetition frequency of 2 Hz.

LV pulse of 300 V for a duration of 50 ms at $t_{\text{LV-sep}}$ ms before the next HV pulse i.e. if $t_{\text{LV-sep}} = 0$ ms then the LV pulse is attached to the next HV pulse which is the same situation as shown in figure 11(e). An LV pulse duration of 50 ms was chosen because this is a sufficient time to pull all negative ions in the discharge gap towards the HV pin electrode.

Figure 15 shows a collection of histograms of t_{inc} for different values of $t_{\text{LV-sep}}$. We see that for small values of $t_{\text{LV-sep}}$ (5–10 ms, figures 15(b) and (c)) a peak is moving from small t_{inc} to higher t_{inc} and for high values of $t_{\text{LV-sep}}$ (150–250 ms, figures 15(e) and (f)) the histogram resembles the baseline experiment histogram (figure 15(a)). We can make sense of this behaviour by noting that the 50 ms LV pulse of 300 V not only pulled all negative ions towards the HV pin electrode, but also pushed positive ions away from it. When the applied potential is now turned off, the separation of these charged species can create an electric field which pulls the charged species back towards their starting position.

If $t_{\text{LV-sep}}$ is not long enough (5–10 ms, figures 15(b) and (c)) we see that the negative ions did not have enough time to return back to their starting position and are still relatively close to the HV pin electrode. Because they are still close to the HV pin electrode they can trigger a discharge quickly (μs) after the application of the HV pulse. If $t_{\text{LV-sep}}$ is long enough (150–250 ms, figures 15(e) and (f)) we can see that the charged species were able to return back to their starting position since the histograms now resemble the baseline experiment (figure 15(a)).

5.5.5. Increasing LV pulse duration. In this section we investigate the influence of high values of $t_{\text{LV-dur}}$ (≥ 50 ms) for the same voltage configuration as for the experiment in figure 11. Figures 11 and 16 show that for $t_{\text{LV-dur}}$ up to 50 ms the third peak moves to the left (the discharge starts faster). For higher values of $t_{\text{LV-dur}}$, the third peak disappears and the second peak seems to re-emerge.

When $t_{\text{LV-dur}} = 50$ ms, the negative ions can gather around the HV pin electrode. When an HV pulse is then applied, right after this LV pulse, the negative ions no longer have to travel towards the HV pin electrode. The only process that needs to happen to trigger a discharge is the detachment of an electron from the negative ion which can then start the discharge.

Increasing $t_{\text{LV-dur}}$ keeps the negative ions against the pin electrode for a longer time. During this time the negative ions can neutralize [45]. Inception becomes slower as $t_{\text{LV-dur}}$ increases since more negative ions are neutralized. The result of applying any positive LV pulse is that negative charges are being removed from the discharge gap. For the LV pulse applied in this work: the free electrons need $t_{\text{LV-dur}} \geq 1$ ms, and the negative ions need $t_{\text{LV-dur}} \geq 50$ ms.

If the LV pulse is on during the entire time between two HV pulses (positive DC bias), we see in figure 16(f) that the third peak is almost completely removed. The counts that are still present around the third peak timescale (125 μs) could still be caused by leftover negative ions, but they can also be due to the long tail of the second peak. The height of the second peak remains relatively unchanged from the base experiment 16(a).

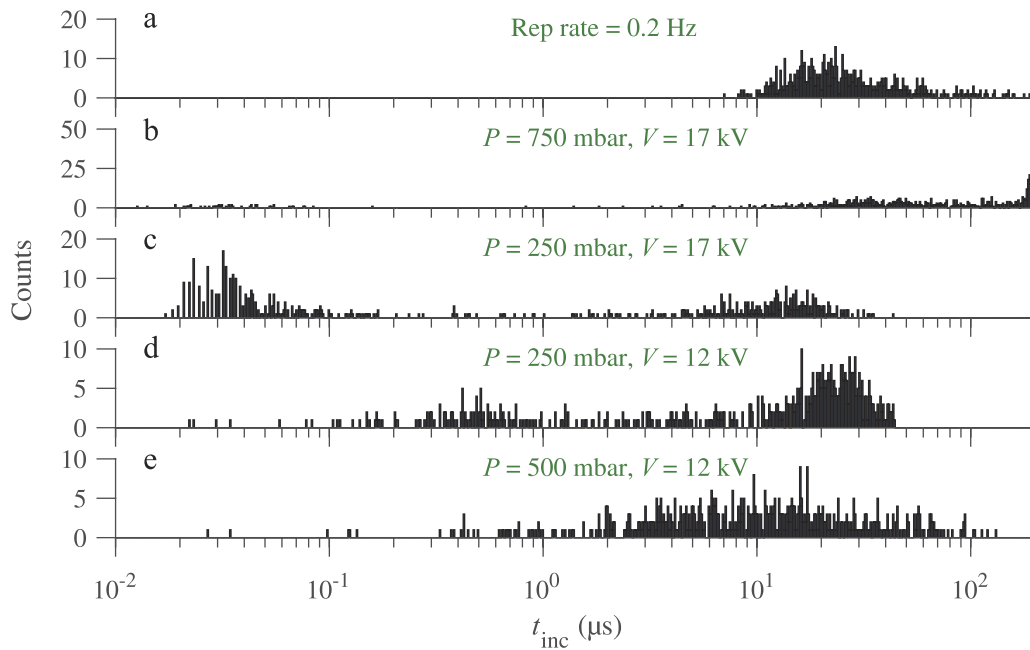


Figure 17. Histograms of discharge inception time t_{inc} for 600 discharges with a different experimental setup than the rest of the experiments. (a) A repetition frequency of 0.2 Hz instead of 2 Hz, (b) A pressure of 750 mbar instead of 500 mbar, (c) A pressure of 250 mbar instead of 500 mbar, (d) A pressure of 250 mbar and HV of 12 kV instead of 500 mbar and 17 kV, (e) an HV of 12 kV instead of 17 kV.

5.6. Streamer inception under different conditions

The experiments described above show that in a specific condition, 17 kV HV amplitude with a repetition frequency of 2 Hz and a working pressure of 500 mbar, an electron which initiates a streamer can originate from three different sources. The question that we now need to address is whether these conclusions are generic or only valid for these specific experiment conditions. Hence, we repeated some of the experiments for combinations of a different repetition frequency (0.2 Hz), pressure (250 and 750 mbar), and voltage (12 kV) to see whether the observations still hold.

Figure 17(a) shows that for a repetition frequency of 0.2 Hz only one peak is present in the t_{inc} histogram. The sources for the first and third peak in figure 9 do not seem to play a role when the repetition frequency is decreased. This may be due to the increased time between HV pulses where no electric field is applied across the gap. During this time ion recombination processes can remove the detaching negative ion species. This again indicates that the source of the second peaks has a long lifetime.

Figure 17(b) shows the t_{inc} histogram for an increased pressure of 750 mbar. We observed similar peaks as in the baseline experiment (figure 9), but the third peak shifted to higher t_{inc} . The drift time of ions will scale inversely with the pressure which can explain the shift of the third peak to higher t_{inc} for a higher pressure. When the pressure is lowered to 250 mbar we see that most inception takes place at $t_{inc} < 0.1 \mu s$. It does not seem reasonable to attribute this shift of t_{inc} from 125 μs to 0.1 μs due to a halving of the pressure. The attachment time would also not be decreased enough to allow for free electrons to exist when an HV pulse is applied and thus triggering a fast inception of the discharge. A possible explanation is that the

detaching negative ions are not converted to O_3^- (stable) or neutralized through recombination reactions as quickly. This would result in more detaching negative ions to remain from the previous discharge. The density of detaching negative ions would increase over time (also in the ionization zone) which will increase the chance of fast discharge inception.

When a lower HV (12 kV) is applied (still higher than the inception voltage, probability of inception = 100%), the first peak seems to have almost disappeared, as shown in figures 17(c) and (d). This may be caused by the smaller ionization zone around the pin electrode which would reduce the chance of having a detaching negative ion in this zone when an HV pulse is applied. This would reduce the occurrences of fast discharge inception (first peak).

In summary, any change in experimental setup which would change the density and distribution of species in the streamer channel will have an effect on the t_{inc} histogram. Parameters that can be changed and will have an influence are: gap distance, applied voltage, gas pressure, repetition frequency, etc.

6. Summary and open questions

We investigated the inception process of repetitive pulsed discharges by measuring the distribution of discharge inception times t_{inc} after the start of the HV pulse. We applied 17 kV pulses of 10 ms duration with a repetition frequency of 2 Hz–500 mbar synthetic air and produced a histogram of inception times t_{inc} , which shows three distinct peaks. By applying LV pulses between the HV pulses, these peaks could be shifted in time or changed in magnitude. We provide theoretical arguments and numerical calculations aimed at identifying differ-

ent electron producing processes that would explain each peak. However, open questions remain.

We start with two theoretical considerations.

First, in section 5.2 it is argued that a single uniformly distributed electron source would create only one early peak, with an initial increase related to the voltage rise time or to the electron detachment time from an oxygen ion, and then with a continuous decay of the inception probability in time. So the different peaks suggest different physical mechanisms.

Second, after a streamer discharge in synthetic air, electrons attach to oxygen molecules on a time scale of 10–100 ns between the HV pulses, and the negative oxygen ions can rapidly detach electrons and start a discharge in the high field zone near the electrode during the next HV pulse. We estimate the O_2^- density in a decaying streamer channel as 10^5 cm^{-3} at the beginning of the next HV pulse. This number is based on the assumption of fast electron attachment to form O_2^- , and on diffusion and recombination of positive and negative ions. However, to reach inception times comparable to experiment, the O_2^- density needs to be as low as 10 cm^{-3} , i.e., 4 orders of magnitude smaller. A possible explanation is that more plasma chemistry has to be added, in particular, that further ion conversion takes place to form the ozone ion O_3^- and NO_3^- . These ions are rather stable, and therefore an effective electron sink. This question needs further investigation in the future.

Concerning the physical processes causing the distinct peaks, we find that the first and the third peak are susceptible to LV pulses, consistent with the drift of negative oxygen ions; in the high field zone near the electrode these ions can detach an electron and create an ionization avalanche. However, to form these two peaks, the ions need to be quite inhomogeneously distributed. The first peak would be caused by a large ion concentration in the high field zone near the electrode (possibly due to the glow during most of the previous HV pulse), and the third peak would be caused by another large ion concentration starting at a distance of about 1.5 cm from the electrode. However, to create the well separated peaks, the two regions with high ion density would need to be clearly separated by a region with very low ion density. It is not clear how such a concentration profile would arise.

The second peak does not shift in time with an LV pulse, which suggests that this electron source is electrically neutral. A continuous, field independent electron source due to Penning ionization could be an explanation, but the lifetime of the Penning ionizing species $N_2(A)$ and $N_2(a')$ are determined by quenching reactions with O_2 and these have timescales on the order of 10–100 ns which makes Penning ionization an unlikely hypothesis. Another explanation could be the presence of quasi-neutral ion patches which cannot be separated by an LV pulse due to space charge effects. The negative ions in these patches can drift in the HV field towards the pin electrode and initiate a discharge by detaching an electron. It is not clear yet if such quasi-neutral patches would be created by a discharge.

Applying a negative LV pulse did not remove the first peak which we argue to be caused by negative ions close to the pin electrode. Secondary emission from the electrode could happen due to impact of positive ions, but in the electric field

of the LV pulse the kinetic energy of these ions would be much lower than the work function of the electrode material. Other secondary emission reactions will need to be investigated in the future to understand this observation better.

The open questions which arose from this research are listed as follows:

- If the first peak is caused by detaching O_2^- -ions, why can it be removed by applying a positive LV pulse? O_2^- -ions from further away in the gap should move towards the pin electrode.
- If the first peak is caused by detaching O_2^- -ions, why can it not be removed by applying a negative LV pulse (or even a negative DC bias)?
- What causes the second peak? It seems to not be influenced by any LV pulse applied. It is the only peak present when the repetition frequency is decreased to 0.2 Hz. It accounts for 61% of the discharge inceptions.
- Simulations show that the third peak can be produced by an inhomogeneous O_2^- -ion distribution. What causes this spatial inhomogeneity?

Acknowledgments

This project has received funding from the European Union's Horizon 2020 research and innovation programme under Project ID 722337 (SAINT).

Appendix A. Analytic estimate for inception probability

In this appendix, we derive an analytic estimate for the probability of inception when only drift is taken into account; effects due to reactions, diffusion or space charge are neglected.

Suppose that a single O_2^- ion or electron is present in the discharge vessel, with a spatially homogeneous probability distribution. For simplicity, we assume that inception occurs when this particle reaches the HV electrode (for the O_2^- ion, an electron would be liberated through detachment in the high field around the electrode). The probability of inception is then equal to the probability that the particle has reached the HV electrode in a time t , which we denote by $F_1(t)$.

As discussed in section 5.2, we can assume the particle flux (or its probabilistic equivalent) to be constant in time until boundary effects due to the finite vessel size become relevant. The underlying assumptions are that the field is divergence-free, that the mobility is constant, and that the initial density is homogeneous. If the flux is constant, then we have $F_1(t) \propto t$. If we assume that any particle reaches the HV electrode within a time t_{\max} , then we can write

$$F_1(t) = t/t_{\max}, \quad (\text{A.1})$$

in other words, the inception probability linearly increases with time from zero to one. If there are N initial particles, the probability of inception $F(t)$ is one minus the probability that inception did *not* occur

$$F(t) = 1 - (1 - F_1(t))^N,$$

so that the probability density of inception $f(t)$ is

$$f(t) \equiv \partial_t F(t) = N(1 - F(t))^{N-1} \frac{dF(t)}{dt}.$$

Plugging in equation (A.1), the result is

$$f(t) = N/t_{\max}(1 - t/t_{\max})^{N-1}. \quad (\text{A.2})$$

For large N and $t/t_{\max} \ll 1$, this can be approximated by $f(t) \approx k(1 - kt)$, where $k = N/t_{\max}$. To a good approximation, the dependence on k instead of N and t_{\max} individually also holds at later times. This means that the specific values used for N and t_{\max} are not important, only their ratio. One could for example consider a volume around the electrode containing $N \gg 1$ initial particles, and let t_{\max} denote the maximal drift times of these particles to the electrode.

ORCID iDs

S Mirpour  <https://orcid.org/0000-0002-4012-1136>
 A Martinez  <https://orcid.org/0000-0002-7826-2348>
 J Teunissen  <https://orcid.org/0000-0003-0811-5091>
 U Ebert  <https://orcid.org/0000-0003-3891-6869>
 S Nijdam  <https://orcid.org/0000-0002-1310-6942>

References

- [1] Morrow R and Lowke J 1997 *J. Phys. D: Appl. Phys.* **30** 614
- [2] Akiyama H 2000 *IEEE Trans. Dielectr. Electr. Insul.* **7** 646–53
- [3] Van Veldhuizen E and Rutgers W 2002 *J. Phys. D: Appl. Phys.* **35** 2169
- [4] Ebert U, Nijdam S, Li C, Luque A, Briels T and van Veldhuizen E 2010 *J. Geophys. Res. Space Phys.* **115** A00E43
- [5] Nijdam S, van de Wetering F M J H, Blanc R, van Veldhuizen E M and Ebert U 2010 *J. Phys. D: Appl. Phys.* **43** 145204
- [6] Bonaventura Z, Bourdon A, Celestin S and Pasko V P 2011 *Plasma Sources Sci. Technol.* **20** 035012
- [7] Shashurin A, Shneider M N and Keidar M 2012 *Plasma Sources Sci. Technol.* **21** 034006
- [8] Nijdam S, Teunissen J, Takahashi E and Ebert U 2016 *Plasma Sources Sci. Technol.* **25** 044001
- [9] Nijdam S, Teunissen J and Ebert U 2020 The physics of streamer discharge phenomena submitted to Plasma Sources Science and Technology (arXiv:2005.14588)
- [10] Okano D 2013 *Rev. Sci. Instrum.* **84** 024702
- [11] Wang Z and Geng Y 2017 *AIP Adv.* **7** 115115
- [12] Van Veldhuizen E and Rutgers W 2003 *J. Phys. D: Appl. Phys.* **36** 2692
- [13] Briels T, van Veldhuizen E and Ebert U 2008 *IEEE Trans. Plasma Sci.* **36** 908–9
- [14] Meek J M 1940 *Phys. Rev.* **57** 722–8
- [15] Montijn C and Ebert U 2006 *J. Phys. D: Appl. Phys.* **39** 2979
- [16] Petersen D, Bailey M, Beasley W H and Hallett J 2008 *J. Geophys. Res. Atmos.* **113** D17205
- [17] Dubinova A, Rutjes C, Ebert U, Buitink S, Scholten O and Trinh G T N 2015 *Phys. Rev. Lett.* **115** 1079–7114
- [18] Kunhardt E and Tzeng Y 1988 *Phys. Rev. A* **38** 1410
- [19] Pancheshnyi S 2013 *J. Phys. D: Appl. Phys.* **46** 155201
- [20] Lowke J 1992 *J. Phys. D: Appl. Phys.* **25** 202
- [21] Li Y, Van Veldhuizen E M, Zhang G J, Ebert U and Nijdam S 2018 *Plasma Sources Sci. Technol.* **27** 125003
- [22] Fengbo T, Qiaogen Z, Bo G, Hu W and Zhou L 2008 *Plasma Sci. Technol.* **10** 588
- [23] Zhao Z and Li J 2019 *Plasma Sources Sci. Technol.* **28** 115019
- [24] Teunissen J and Ebert U 2016 *Plasma Sources Sci. Technol.* **25** 044005
- [25] Cross J and Beattie J 1980 *Can. Electr. Eng. J.* **5** 22–32
- [26] Giao T N and Jordan J B 1968 *IEEE Trans. Power Appar. Syst.* **87** 1207–15
- [27] Pancheshnyi S 2005 *Plasma Sources Sci. Technol.* **14** 645–53
- [28] Wormeester G, Pancheshnyi S, Luque A, Nijdam S and Ebert U 2010 *J. Phys. D: Appl. Phys.* **43** 505201
- [29] Popov N A 2010 *Plasma Phys. Rep.* **36** 812–8
- [30] 2020 *Itikawa Database* www.lxcat.net
- [31] Itikawa Y 2006 *J. Phys. Chem. Ref. Data* **35** 31–53
- [32] Itikawa Y 2009 *J. Phys. Chem. Ref. Data* **38** 1–20
- [33] 2020 *Phelps Database* www.lxcat.net
- [34] Kossyi I A, Kostinsky A Y, Matveyev A A and Silakov V P 1992 *Plasma Sources Sci. Technol.* **1** 207–20
- [35] Zheleznyak M B and Mnatsakanyan A K 1982 *High. Temp.* **20** 357–62 <http://mi.mathnet.ru/eng/tvt6325>
- [36] Chanrion O and Neubert T 2008 *J. Comput. Phys.* **15** 7222–45
- [37] Viehland L A and Kirkpatrick C C database 2019 *VIEHLAND Database* www.lxcat.net
- [38] *COMSOL Multiphysics® version 5.4* COMSOL AB stockholm www.comsol.com
- [39] Rutjes C 2018 Modeling high energy atmospheric physics and lightning inception *PhD Thesis* Department of Applied Physics proefschrift
- [40] Hagelaar G J M and Pitchford L C 2005 *Plasma Sources Sci. Technol.* **14** 722–33
- [41] *Bolsig- solver version linux 03/2016* <http://www.bolsig.laplace.univ-tlse.fr/>
- [42] Lowke J 2015 *J. Geophys. Res. Atmos.* **120** 3183–90
- [43] Guerra V and Loureiro J 1997 *Plasma Sources Sci. Technol.* **6** 361–72
- [44] Capitelli M, Ferreira C M, Gordiets B F and Osipov A I 2000 *Plasma Kinetics in Atmospheric Gases (Springer Series on Atomic, Optical, and Plasma Physics)* (Berlin: Springer)
- [45] Varnerin L J 1953 *Phys. Rev.* **91** 859–63